Dynamic modeling of in vitro lipid digestion: Individual fatty acid release and bioaccessibility kinetics

Thuy Minh Giang, Sebastien Gaucel, Pierre Brestaz, Marc Anton, Anne Meynier, Ioan-Cristian Trelea, Steven Le Feunteun

Dynamic modeling of *in vitro* lipid digestion: Individual fatty acid release and bioaccessibility kinetics

T.M. Giang[1,2], S. Gaucel[1,2], P. Brestaz[3], M. Anton[3], A. Meynier[3], I.C. Trelea[1,2] and S. Le Feunteun*[1,2]

[1] INRA, UMR782 Génie et Microbiologie des Procédés Alimentaires, F-78850 Thiverval Grignon, France

[2] AgroParisTech, UMR782 Génie et Microbiologie des Procédés Alimentaires, F-78850 Thiverval Grignon, France

[3] INRA, UR1268 Biopolymères Interactions Assemblages, F-44300 Nantes, France

***Corresponding author**: steven.le-feunteun@grignon.inra.fr, +33(0)13814596

Abstract

The aim of this study was to gain knowledge about the role of triacylglycerol (TAG) composition in fatty acids (FA) of o/w emulsions on both the pancreatic lipolysis kinetics and the bioaccessibility of released products (i.e. contained within the bile salt micellar phase). A mathematical model was developed and its predictions were compared to a set of experimental data obtained during an *in vitro* digestion of a whey protein stabilized emulsion. Modeling results show that FA residues of TAG were hydrolyzed at specific rates, inducing different bioaccessibility kinetics. The estimated lipolysis rate constants of the studied FA (C8:0, C10:0 >> C18:1 n-9 >> C12:0 > C14:0 > C16:0 ≈ C16:1 n-7 > C22:6 n-3) were in close agreement with the available literature on the substrate specificity of pancreatic lipase. Results also suggest that lipolysis products are very rapidly solubilized in the bile salt mixed micelles with no fractionation according to the FA carbon chain.

Keywords: Emulsion, Digestion, Pancreatic lipase, Substrate specificity, DHA, Simulation.

1. Introduction

Human digestion of lipid emulsion is influenced by both physiological parameters and emulsion properties. Triacylglycerol (TAG) digestion occurs essentially in the intestine where about 80% of the lipolysis reaction take place (Carriere, Barrowman, Verger, & Laugier, 1993). The reaction is mediated by the pancreatic lipase-colipase complex at the oil-water interface and releases the *sn*-2-monoacylglycerol (MAG) and two free fatty acids (FFA) (Golding & Wooster, 2010). Lipolysis products are then incorporated into bile salt micelles before being transported to the gut wall and absorbed by the organism (Smith & Morton, 2010). Hence, physiological parameters such as the concentrations of pancreatic lipase, colipase and bile salts can all modify lipid digestion. The structural characteristics of emulsions are also important to consider when evaluating lipolysis kinetics. For instance, the nature of emulsifiers influences the properties of the oil-water interface and can therefore affect lipase adsorption onto droplets. The size of the oil droplets is another key parameter since fine emulsions with high interfacial areas facilitate the enzyme activity compared to coarse emulsions with low interfacial areas (Armand et al., 1999; Golding & Wooster, 2010; Li & McClements, 2010).

The TAG composition in fatty acid residues (FA), characterized by their carbon chain length and degree of unsaturation, also has a strong impact. Several studies have demonstrated that human and porcine pancreatic lipases exhibit a certain fatty acid specificity (Berger & Schneider, 1991; Desnuelle & Savary, 1963; Mukherjee, Kiewitt, & Hills, 1993; Yang, Kuksis, & Myher, 1990). For instance, it is well known that pancreatic lipase is more active on medium chain TAG (MCT, up to C10) than on long chain TAG (LCT, from C12) (Armand et al., 1992; Desnuelle & Savary, 1963; Golding et al., 2011; Li & McClements, 2010), and that its activity depends on the number and positions of unsaturations (Mukherjee et al., 1993; Yang et al., 1990). Long chain polyunsaturated fatty acids, such as docosahexaenoic acid

(C22:6 n-3, DHA), have also been reported to be among the most resistant FA to pancreatic lipase (Bottino, Vandenburg, & Reiser, 1967; Yang et al., 1990), possibly because of the short distance of the first double bond from the ester linkage (Akanbi, Sinclair, & Barrow, 2014; Bottino et al., 1967; Lawson & Hughes, 1988).

Moreover, the extent of FFA and MAG that can be solubilized into the bile salt micelles also seems to be product dependent (Freeman, 1969; Hofmann, 1963). For instance, the molar saturation ratio (mole of incorporated products/mole of bile salts) in a sodium glycodeoxycholate solution at 37°C has been reported to vary from 0.07 for stearic acid (C18:0) to 1.86 for lauric acid (C12:0) with intermediate values for long chain unsaturated FFA such as oleic (C18:1 n-9) and linoleic acids (C18:2 n-6) (Freeman, 1969). Such values, which can be partly reasoned in terms of molecular polarities and amphiphilic properties, are however dependent on numerous parameters such as the type of bile acid used or the pH of the solution (Freeman, 1969; Hofmann, 1963). Moreover, if the addition of *sn*-1-monoolein within the bile salt solution has been reported to improve the bile salt solubility of FFA, the opposite has been observed with the addition of oleic acid (Freeman, 1969). Given the variety of lipolysis products and bile acids that coexist during the intestinal digestion of edible oil, it therefore seems difficult to predict the bioaccessibility of lipolysis products.

Modeling has proven to be a powerful tool for a better understanding of the intestinal digestion kinetics. Various models of lipid digestion have been published over the last decades. Several models are based on the Michaelis-Menten equation. Verger and co-workers were the first to adapt such approach to the biphasic nature of the lipolysis reaction by taking into account the interfacial concentrations of the substrates and enzymes (Verger & de Haas, 1976; Verger, Mieras, & de Haas, 1973). Several variants have been proposed since, as for instance by Jurado, Camacho, Luzón, Fernández-Serrano, & García-Román (2008) for a bacterial lipase. These models are however quite complex and often require parameter values

that are difficult to determine experimentally, in particular for the digestion of edible oils composed of different TAG species. In a much simpler approach, intestinal lipolysis can also be described by a first order kinetic model (Ye, Cui, Zhu, & Singh, 2013). If such models can be useful in comparing the initial enzyme activity in different conditions, they do not take into account the interfacial area of oil droplets. This is why Li & McClements (2010) proposed a model in which the rate constant is expressed per unit of interfacial area, and that accounts for a progressive decrease of the oil droplet size. This model provided good fits of pH-stat measurements performed on different emulsions with the assumptions that the number of droplet remains unchanged and all droplets have the same size at any given time. Recently, we resorted to a similar modeling approach to show, by integrating experimentally measured droplet sizes, that the reduction of the interfacial area induced by droplet coalescence was the main reason why our *in vitro* intestinal lipolysis seemed to stop before the substrate was fully exhausted (Giang et al., 2015).

Nevertheless, all the above models assume a unique reaction rate constant without considering the FA composition of the studied oils. Hence, they cannot be used to reproduce the release kinetics of individual FA. In the present study, we develop a mathematical model of intestinal lipolysis that takes the composition of the oil substrate into account. It predicts the lipolysis kinetics of each FA residue and their *in vitro* bioaccessibility, defined as the concentration of FA (FFA + *sn*-2-MAG) measured within the bile salt micellar phase. The model is applied to a set of experimental data measured during the *in vitro* gastro-intestinal digestion of a whey protein stabilized emulsion. The estimated values for the model parameters (FA specific lipolysis rate constants and bile salt micellar fractions) are compared with the available literature and discussed according to their biochemical meanings.

2. Material and method

105 2.1. Materials

106 The oil containing medium-chain triacylglycerols (MCT), Miglyol 812S, was purchased from
107 Sasol GmbH, Germany. The main fatty acids contained in this oil were C8:0 (54% w/w) and
108 C10:0 (43%). The oil containing long-chain triacylglycerols (LCT), DHAsco, was obtained
109 from Martek, via DSM Nutritional Products Ldt, Switzerland. It contained docosahexahenoic
110 acid (DHA, C22:6 n-3) as major fatty acid (40% w/w) along with C12:0 (4%), C14:0 (12%),
111 C16:0 (12%) and C18:1 n-9 (24%). Whey protein powder (Prolacta 95) was purchased from
112 Lactalis Ingredients, France. Pepsin (P7012, 2,500 U mg^{-1}), mucin (M2378), pancreatin
113 (P7545, 8×USP specifications), pancreatic lipase (L3126, 120 U mg^{-1}) and bile extract (B8631)
114 were from porcine origin and obtained from Sigma-Aldrich, France. Water was Milli-Q water.
115 Solvents for liquid chromatography were chloroform for HPLC (Carlo Erba), methyl alcohol
116 for HPLC (99.9%, Carlo Erba) and ammonia solution (30%, Carlo Erba). Acetone (Pure RE,
117 Carlo Erba), sulfuric acid (RPE 96%, Carlo Erba), cyclohexane and heptadecanoic acid
118 (Sigma) were used for the preparation of fatty acid methyl esters (FAME) of the micellar
119 phase during intestinal digestion.

120

121 2.2. Emulsion preparation and digestion

122 A whey protein stabilized emulsion with droplet diameters below 1 μm was first prepared
123 according to the procedure previously described in Giang et al. (2015). Briefly, the oil phase
124 (20% w/w) contained 37.5% (w/w) of MCT and 62.5% of LCT, and the aqueous phase (80%
125 w/w) contained 4% (w/w) of whey protein powder, used as emulsifier, in a 0.1M sodium
126 phosphate buffer (pH 7.0). After high pressure homogenization and addition of maltodextrin
127 solution to improve the freeze-dried stability of oil droplets, the emulsion was freeze-dried.
128 On the day of the *in vitro* experiments, the dry emulsion was rehydrated in Milli-Q water to
129 obtain a final oil concentration of 3.2% (w/w).

A volume of 3 mL of the rehydrated emulsion, corresponding to an oil mass of about 96 mg, was placed into hermetically sealed headspace vials (22.4 mL). The gastric and intestinal phases of the *in vitro* digestion experiments were performed sequentially at 37°C under magnetic stirring (400 rpm). The gastric phase duration was 60 min and was launched by adding 2.12 mL of simulated gastric fluid (SGF) and 40 µL of 1M HCl to reach a final pH of 2.5. The SGF solution contained 3.9 g L^{-1} of pepsin (corresponding to 10,000 U per mL of SGF using hemoglobin as substrate), 2.4 g L^{-1} of mucin, 120 mM of NaCl, 2 mM of KCl and 6 mM of $CaCl_2$. The intestinal phase duration was then launched for 300 min maximum by adding 4.86 mL of simulated intestinal fluid (SIF) and 100 µL of 1M $NaCO_3$ to reach a final pH of 6.5. The SIF solution contained 30.8 g L^{-1} of bile extract powder, 0.82 g L^{-1} of pancreatin (activity: 8×USP specifications), 0.41 g L^{-1} of pancreatic lipase (corresponding to 100 U per mL of SIF using olive oil as the substrate), and the same electrolyte concentrations as the SGF.

Samples were taken at t = 0 min of the intestinal phase using a modified SIF that contained all constituents except pancreatin and lipase, and at 15, 30, 60, 120 and 300 min of intestinal digestion. One vial was used for one sampling time and one type of measurement (quantification of LCT and MCT by HPLC, quantification of the lipolysis products within the bile salt micellar phase by GC, or droplet size by laser granulometry) so that the contents of 18 vials in total were analyzed (3 methods times 6 sampling times) for one digestion. Three independent digestion experiments, further denoted as replicates, were performed.

2.3. Quantification of LCT and MCT by HPLC

HPLC paired with an evaporative light scattering detector (ELSD) was used to quantify the decrease in both LCT and MCT masses during the time course of the *in vitro* digestions. Total lipids were extracted according to Bligh and Dyer method with minor modifications in the

ratio $CHCl_3/CH_3OH/H_2O$ 1/2/1, and dissolved in $CHCl_3$ to obtain a final lipid concentration of 0.7 mg mL^{-1}. HPLC operating conditions were similar to those described in Kenmogne-Domguia, Meynier, Viau, Llamas, & Genot (2012) using a Uptip-prep Strategy column (2.2 µm SI, 150×4.6 mm, Interchim, Montluçon, France) and 30 µL of injected lipid extract. The signal of LCT and MCT (retention times of 1.21 and 1.32 min, respectively) were deconvoluted using a specifically developed algorithm running with the Matlab™ software (The MathWorks Inc., Natick, MA), and converted into masses using a pre-established calibration curve. LCT and MCT masses were finally converted into lipolysis percentages using Equation 1:

$$lipolysis\ (t) = \frac{m_{TAG_0} - m_{TAG}(t)}{m_{TAG_0}} \times 100\ \% \qquad (1)$$

where m_{TAG_0} and $m_{TAG}(t)$ are the masses (mg) of LCT or MCT initially present in the vials and measured by HPLC at time t, respectively.

2.4. Droplet size measurement

The volume-based distribution of oil droplet sizes was measured using a Mastersizer S (Malvern Instruments Ltd., Worcestershire, UK) equipped with a 2 mW He-Ne laser of λ = 633 nm and the 300RF lens with detection limits of 0.05 and 900 µm. The refractive index n_0 of the aqueous phase was 1.33 and the properties of the dispersed phase were 1.457 for the refractive index and 0.001 for the absorption. Samples were diluted with distilled water to reach an oil volume concentration near 0.01% (w/w) for the circulation in the measurement cell. The surface weighted mean diameter, d_{32}, was calculated using Equation 2:

$$d_{32} = \frac{\sum n_i^3 d_i^3}{\sum n_i^2 d_i^2} \qquad (2)$$

where n_i is the number of droplets of diameter d_i.

177 2.5. Quantification of lipolysis products within the bile salt micellar phase by GC

178 Intestinal aliquots were frozen immediately after sampling. The day after, they were
179 centrifuged at 50,000 rpm for 45 min at 4°C with Aventi J26-XP (Beckman-Coulter). Three
180 phases were observed after centrifugation: a lipidic phase at the top, a pellet at the bottom,
181 and a major intermediate phase containing the bile salt mixed micelles and which will be
182 further referred as the micellar phase. 500 µL of the micellar phase were sampled for the
183 determination of its FA composition by direct trans-methylation as described previously by
184 Berton, Genot, & Ropers (2011). Briefly, 500 µL of the micellar phase was trans-methylated
185 in presence of 100 µL of internal standard (heptadecanoic acid 1mg/mL in acetone/MeOH 2/1
186 v/v). 2 mL of methanol and 400 µL of H_2SO_4 were then introduced. The mixture was mixed;
187 the tube screw capped and then heated à 100°C for 1 h. After cooling at room temperature,
188 500 µL of water and 1 mL of cyclohexane were added. After mixing, and decantation, the
189 organic phase was removed for later analysis by GC. Fatty acid methyl ester (FAME)
190 analyses were performed on a gas chromatograph paired with a splitless injector and a FID
191 (Clarus, Perkin Elmer). They were separated on a capillary column (DB 225, 30 m X 0.25
192 mm, film thickness 0.25 mm) after splitless injection. The carrier gas (H_2) was set at 2 m min^{-1}.
193 Temperature gradient was programmed as follows: 50°C for 3 min, increase to 180°C at
194 15°C min^{-1}, 7 min at 180°C, increase to 220°C at 10°C min^{-1} and finally 10 min at 220°C. The
195 temperature of the injector and the detector were maintained at 250°C. Individual FA were
196 identified by comparison of their retention time with those of standards FAME mix (cat
197 47885-U 37, Supelco); n-3 PUFA from menhaden oil (cat 4-7085 U-14, Supelco), and marine
198 oil standard of the AOCS. Peak surfaces were integrated and corrected by response factors of
199 individual fatty acids.

200 The FA composition of the native emulsion was also quantified by GC. As summarized in
201 Table 1, 8 fatty acids representing 95.6% of the total FA mass, were considered for the

modeling approach: C8:0, C10:0, C12:0, C14:0, C16:0, C16:1 n-7, C18:1 n-9, and C22:6 n-3. These 8 FA showed coefficients of variation of less than 10.26% over the three replicate measurements. Since the emulsion was prepared from a mixture of two oils, the last 2 columns of Table 1 provide the fractional contributions of LCT (α_{FA_i}) and MCT (1-α_{FA_i}) for each FA residue. Results show that almost all C8:0 and C10:0 came from the MCT oil, whereas all the other fatty acids came essentially from LCT. These fractions will be used for TAG mass calculations in the model.

3. Mathematical modeling

3.1. Model assumptions and equations

The model was built to predict the lipolysis kinetics and the concentration profiles of the lipolysis products in the bile salt micellar phase, knowing that pancreatic lipase produces two FFA and one *sn*-2-MAG per TAG molecule. However, if the GC analyses of the samples make it possible to quantify the different acyl chains, they cannot be used to discriminate their molecular origin, *i.e.* free or esterified fatty acids. In the rest of this paper, the term fatty acid (FA) will therefore refer to FA carbon chains in any kinds of molecular products. The main modeling assumptions were as follows:

A1: the hydrolysis rate of a given fatty acid residue FA_i was independent of the *sn*-position within TAG molecules, with FA_i referring to the fatty acid considered (C8:0, C10:0, C12:0, C14:0, C16:0, C16:1 n-7, C18:1 n-9, or C22:6 n-3).

A2: the hydrolysis rate of a given fatty acid residue FA_i was proportional to the interfacial area occupied by this acyl chain.

$$\frac{dm_{FA_i}^{lip}(\mathrm{t})}{dt} = -k_{FA_i}.A_{FA_i}(t) \qquad (3)$$

where $m_{FA_i}^{lip}$ is the mass of FA_i in the oil droplets (mg), k_{FA_i} is the lipolysis rate constant of FA_i (mg m^{-2} min^{-1}), and $A_{FA_i}(t)$ is the interfacial area occupied by FA_i (m^2) at time t (min).

A3: the interfacial area occupied by FA_i at time t was assumed to be proportional to its molar fraction within the oil droplets.

$$A_{FA_i}(t) = \frac{n_{FA_i}^{lip}(t)}{\sum_i n_{FA_i}^{lip}(t)} . A_{TAG}(t) \qquad (4)$$

where $n_{FA_i}^{lip}(t)$ is the number of moles of FA_i in the oil droplets (mol) at time t and A_{TAG}(t) is the interfacial area of oil droplets (m^2) at time t. This equation can be rewritten as

$$A_{FA_i}(t) = \frac{\frac{m_{FA_i}^{lip}(t)}{M_{FA_i}}}{\sum_i \frac{m_{FA_i}^{lip}(t)}{M_{FA_i}}} . A_{TAG}(t) \qquad (5)$$

where M_{FA_i} is the molar mass of FA_i (g mol^{-1}).

A4: oil droplets in the emulsion were considered as spheres. The droplet interfacial area is thus:

$$A_{TAG}(t) = 6.\frac{m_{TAG}(t)}{\rho . d_{32}(t)} \qquad (6)$$

where $m_{TAG}(t)$ is the total mass (mg) of TAG at time t, ρ is the mean mass density of the TAG (taken as 0.92 mg mm^{-3}) and $d_{32}(t)$ is the surface weighted mean droplet diameter measured by laser diffraction (nm).

Combining assumptions A1-A4, Eq. (3) can be rewritten:

$$\frac{dm_{FA_i}^{lip}}{dt} = -k_{FA_i} \frac{\frac{m_{FA_i}^{lip}(t)}{M_{FA_i}}}{\sum_i \frac{m_{FA_i}^{lip}(t)}{M_{FA_i}}} . 6.\frac{m_{TAG}(t)}{\rho . d_{32}(t)} \qquad (7)$$

A5: our experimental results show that only a fraction of hydrolyzed products were transferred into the bile salt micellar phase. To calculate the masses of FA_i within this phase, a "micellar fraction", $f_{FA_i}^{mic}$, was therefore introduced with the assumption that the transfer of lipolysis products into the micellar phase is instantaneous:

$$\frac{dm_{FA_i}^{mic}}{dt} = -f_{FA_i}^{mic}\frac{dm_{FA_i}^{lip}}{dt} \qquad (8)$$

where $m_{FA_i}^{mic}$ is the mass of FA_i in the micellar phase (mg).

The micellar fraction $f_{FA_i}^{mic}$ and the lipolysis rate k_{FA_i} are the unknown parameters of the model. They were estimated for each FA_i by adjusting the model to the experimental data (see section 3.2). To this end, model predictions for TAG masses were calculated as follows.

The total TAG mass, $m_{TAG}(t)$, is the sum of the medium chain TAG (MCT) and long chain TAG (LCT) masses:

$$m_{TAG}(t) = m_{\mathrm{MCT}}(t) + m_{\mathrm{LCT}}(t) \qquad (9)$$

where $m_{MCT}(t)$ and $m_{LCT}(t)$ are the MCT and LCT masses (mg) at time t, respectively, calculated according to their fractional mass contributions ($\alpha_{\mathrm{FA_i}}$ and 1- $\alpha_{\mathrm{FA_i}}$) shown in Table 1 and by adding the adequate mass of glycerol moiety:

$$m_{\mathrm{MCT}}(t) = \sum\nolimits_{\mathrm{i}} m_{FA_i}^{lip}(t)\,.\,(1-\alpha_{FA_i}) + m_{Glycerol_{MCT}}(t) \qquad (10)$$

$$m_{\mathrm{LCT}}(t) = \sum\nolimits_{\mathrm{i}} m_{FA_i}^{lip}(t)\,.\,\alpha_{FA_i} + m_{Glycerol_{LCT}}(t) \qquad (11)$$

where $m_{Glycerol_{LCT}}(t)$ and $m_{Glycerol_{MCT}}(t)$ are the masses of glycerol moiety coming from MCT and LCT, respectively. They were calculated via a molar balance equation by considering that there is one mole of glycerol moiety per three moles of FA_i.

3.2. Parameter estimation

256 The differential equations of the model (Eq. 7 and Eq. 8) were solved numerically using
257 Matlab® software (The MathWorks Inc., Natick, MA) equipped with the Statistics Toolbox.
258 The surface weighted mean diameter $d_{32}(t)$ was integrated into the model using linear
259 interpolations of the experimental values. Model outputs, namely the evolution of the MCT
260 and LCT masses and masses of hydrolyzed products within the micellar phase, were
261 confronted to the corresponding experimental results measured by HPLC and GC,
262 respectively, to estimate the unknown model parameters: k_{FA_i} and $f_{FA_i}^{mic}$. Standard errors,
263 coefficients of variation and 95% confidence intervals of the estimated parameter values were
264 computed using the nonlinear regression software in the Matlab® Statistics Toolbox and it
265 was checked that estimated values were statistically significant at 0.05 level.
266
267 **4. Results and Discussion**
268 4.1. Experimental results
269 Results related to the evolution of droplet sizes during the gastric and intestinal phases were
270 described in detail previously (Giang et al., 2015). It was found that droplet flocculation took
271 place during the gastric phase but these aggregates where re-dispersed after the subsequent
272 addition of bile. Fig. 1 summarizes the results related to the evolution of oil droplet sizes
273 (d_{32}) during the intestinal phase together with the corresponding TAG lipolysis kinetics. Fig.
274 1A shows that the lipolysis rate was much higher for MCT than for LCT as the hydrolysis of
275 MCT was completely finished after 15 min, whereas about 20% of LCT could still be
276 detected after 300 min of intestinal digestion. In good agreement with many studies (Li &
277 McClements, 2010; Ye et al., 2013; Zhu, Ye, Verrier, & Singh, 2013), the LCT lipolysis
278 curve also showed two stages with a fast initial reaction rate that markedly slowed down after
279 about 30 min. As previously shown in (Giang et al., 2015), this can be attributed to the sudden
280 increase of the surface weighted mean diameter induced by the coalescence of oil droplets,

and which led to a sharp reduction of the interfacial area available for lipase adsorption (Fig. 1B).

Fig. 2 presents the bioaccessibility of the 8 fatty acids considered, *i.e.* the lipolysis product concentrations measured within the micellar phase, expressed as percentages of FA initially present in the oil phase. Three main observations can be made. First, fatty acids can be divided into two groups according to the evolution of their bioaccessibility. The first group contains the FA arising from lipolysis of MCT, C8:0 and C10:0. They were released more quickly than the second group which corresponds to the FA arising from the lipolysis of LCT (Table 1). One may also notice that the long chain FA showed two-stage shapes with a slower rate of appearance within the micellar phase after about 30 min. These results are therefore consistent with the MCT and LCT lipolysis kinetics deduced from the HPLC measurements (Fig. 1A). Second, both the rate of appearance and the concentration measured at the end of the experiment (300 min) depended on the FA considered. The rate and extent of FA appearance in the micellar phase tended to be higher for shorter FA. This confirms that all fatty acids do not behave in the same way in terms of lipolysis kinetics and/or incorporation into the bile salt micelles. Finally, since MCT were fully hydrolyzed in less than 15 min according to the HPLC measurements (Fig. 1A), the plateau value of about 65% for C8:0 and C10:0 (Fig. 2) demonstrates that only a fraction of hydrolyzed products was recovered within the micellar phase. This is in accordance with the study of Sek, Porter, Kaukonen, & Charman (2002) who showed that lipolysis products can also be found in the oil and pellet phases after the centrifugation step used to separate the micellar phase.

4.2. Modeling results

The model was designed to simulate the lipolysis kinetics as well as the bioaccessibility of individual FA, and considers 8 fatty acids representing 95.6% of the total FA mass. The

parameters to be estimated were the reaction rate constant (k_{FA_i}) and the micellar mass fraction ($f_{FA_i}^{mic}$) for each FA.

It appeared that the fatty acids coming from MCT, C8:0 and C10:0, were fully hydrolyzed in less than 15 min of intestinal digestion (Fig. 1A and Fig. 2), *i.e.* before the first sampling time. The lipolysis rate constants, k_{C8} and k_{C10}, could therefore not be estimated due to lack of intermediate data. After preliminary model simulations, they were set at the minimum value enabling to reproduce a sufficiently fast MCT lipolysis, which was found to be 10 mg m^{-2} min^{-1}. According to the above considerations, 6 lipolysis rates k_{FA_i} and 8 micellar fractions $f_{FA_i}^{mic}$ remained to be determined. In a first attempt, all parameters were estimated by fitting the model to the experimental data. This model version provided very good fits (data not shown) but it appeared that the $f_{FA_i}^{mic}$ values were similar for all FA except C8:0. In other words, the bile salt solubilization ratio of the lipolysis products was about the same for FA longer than C8:0. To reduce the number of unknown parameters, it was therefore decided to keep only two $f_{FA_i}^{mic}$ parameters, one for C8:0 and the other one common to all the other FA. Hence, the final version of the model had 6 unknown lipolysis rates k_{FA_i} and 2 unknown micellar fractions $f_{FA_i}^{mic}$. Fig. 3 shows that this model version still provided very good fits of the experimental data, and Table 2 shows that the parameter values were properly estimated (coefficients of variation smaller than 10%). These results are further discussed according to their biological meanings.

4.3. Fractions of hydrolyzed products recovered within the bile salt micellar phase

Estimated values for the micellar fraction parameters (Table 2) can be interpreted as follows. About 70% (w/w) of the C8:0 lipolysis products were released in the bile salt micellar phase, and about 56% for the other FA. The remaining amounts of products were retained in the oil and pellet phases during the centrifugation step. The order of magnitude of these values is

consistent with studies in which centrifugation was also employed to measure the micellar content in lipolysis products (Sek et al., 2002). Note also that the model assumes an instantaneous transfer of the products into the micellar phase. The very good fits of the bioaccessiblility kinetics (Fig. 3) obtained under this assumption therefore strongly suggest that the solubilization of the lipolysis products in the bile salt micelles was not rate limiting.

Similar micellar fraction values for all the lipolysis products considered may seem in contradiction with previously published data. Several studies have indeed shown that lipolysis products behave differently in terms of bile salt solubility (Freeman, 1969; Hofmann, 1963), with molar saturation ratios that can vary from 0.07 up to 1.86 (Freeman, 1969). In fact, the experimental protocol used in these studies was quite different from an *in vitro* digestion protocol since mixtures of pure molecules were used to obtain these results. During the digestion of complex natural oils, a great number of interactions take place between the different lipolysis products and bile acids, and this can greatly modify the solubility of the products in the bile salt mixed micelles. In our study, the products/bile salts molar ratio was of about 1.32 at the end of the experiment, thereby indicating that the saturation ratio for our mixture of lipolysis products was even greater.

One may also wonder why the micellar fraction obtained for C8:0 is different from those obtained for the other FA products. This can probably be attributed to the greater water solubility of this fatty acid. Indeed, using the formula proposed by Tzocheva et al. (2012), it was found that C8:0 was the only free fatty acid with a significant water solubility (0.64 g L^{-1}). More precisely, within our experimental conditions, it can be estimated that about 6 mg of caprylic acid could dissolve if our reaction medium was made of pure water. This corresponds to 31% by weight of the total C8:0 mass introduced within the digestive tubes. According to our modeling results, a common micellar fraction of 56% provides good results for all FA except C8:0, for which a micellar fraction of 70% was estimated. The additional 14% for

C8:0 (70 = 56 + 14) are therefore compatible with the contribution of a water soluble fraction, knowing that the micellar phase is not pure water and that the total C8:0 mass accounts for both FFA and *sn*-2-MAG molecular forms. According to this interpretation, the solubility of the lipolysis products in the bile salt mixed micelles would therefore be approximately the same for all the FA considered, C8:0 included.

4.4. FA specific lipolysis rate constants

The lipolysis rate constants estimated with the model are given in Table 2. The same data, but expressed as normalized values relatively to oleic acid, are also presented in Fig. 4 for comparison purposes with the available literature. We may first highlight the very good agreement of our results with those obtained by Berger & Schneider (1991) for C12:0, C14:0, C16:0 and C18:1n-9 in spite of very different experimental conditions. Indeed, if our results arise from the modeling of *in vitro* intestinal digestion of emulsified lipids made of a mixture of different TAG, Berger & Schneider (1991) used a protocol based on a lipase-catalyzed reaction in an organic solvent with a mixture of TAG that contained 3 identical acyl residues. We may also stress that, according to our results, C8:0 and C10:0 presented rate constants that were at least 3 times the one estimated for oleic acid (Table 2), hence confirming the early study of Desnuelle & Savary (1963) who found the highest pancreatic lipase activity for C4:0 and reported a strong decrease in activity (by a factor of about 2) between C10:0 and C12:0. Altogether, our findings are therefore in agreement with the reported tendency of pancreatic lipase to be less active on longer saturated fatty acid residues. These variations are usually ascribed to substrate dependent catalytic lipase activity, although other reaction steps, such as interfacial or diffusive mass transfers of substrates and products, may play a role (Verger & de Haas, 1976; Verger, Mieras, & de Haas, 1973).

Besides, if DHA (C22:6 n-3) was not studied by Berger & Schneider (1991), slower rates of pancreatic lipolysis for long-chain polyunsaturated fatty acids have been reported by many authors (Akanbi et al., 2014; Bottino et al., 1967; Zhu et al., 2013). For instance, the lipolysis rate constant of DHA should be about 0.17 times that obtained for C18:1 n-9 according to Yang et al. (1990), and of about 0.6 times that obtained for C14:0 according to Mukherjee et al. (1993). These values are represented by a triangle and a circle in Fig. 4, respectively, to show that our estimated rate constant for DHA is consistent with these findings. This higher resistance of long-chain polyunsaturated fatty acids has been attributed to an inhibitory effect induced by the presence of a double bond near the carboxyl group (Akanbi et al., 2014; Bottino et al., 1967; Lawson & Hughes, 1988).

4.5. Evolution of the TAG composition during lipolysis

Fig. 5 presents the oil-water interfacial areas occupied by each FA residue of TAG molecules as given by the model. They were calculated by assuming proportionality with their molar concentrations within the lipid phase (Eq. 4). Therefore, the evolution of these FA specific interfacial areas is also representative of the predicted changes of the oil droplet composition during the course of digestion. Results show that about 50% of the oil surface area was occupied by MCT fatty acid residues (C8:0 and C10:0) at the beginning of the experiment. After 15 min, MCT had totally disappeared (Fig. 1A) due to higher lipolysis rate constants for C8:0 and C10:0. This induced a considerable change in the composition of the remaining oil, with only long-chain fatty acid residues remaining. At the end of the experiment, DHA was by far the dominant FA residue (more than 70% by mole) because it had the lowest lipolysis rate constant (Table 2).

As a final remark, we may highlight that our previous model (Giang et al., 2015) assumed an average lipolysis rate for the entire LCT oil fraction, which somewhat overestimated the LCT

lipolysis rate at long times. By taking into account FA specific lipolysis rate constants, the newly developed model predicts an accumulation of most resistant FA residues in the remaining oil (Fig 5), which leads to a progressive decrease of the average reaction rate and a better agreement with experimental measurements of the remaining LCT at 300 min (Fig 3).

5. Conclusion

In the present study, our previous model (Giang et al., 2015) was extended to take into account the fatty acid composition of the oil substrate, and to enable the modeling of the *in vitro* bioaccessibility of the lipolysis products. The model provided very good fits of the experimental data and shows that the differences observed in the bioaccessibility kinetics of the studied FA originated from different FA lipolysis rate constants. It was also used to simulate the compositional evolution of the remaining oil during the course of digestion. Results related to the FA specific reaction rates were in good agreement with the available literature and confirm a general tendency towards a greater pancreatic lipase activity on shorter fatty acid residues. Our results also support the idea that lipolysis products are rapidly and equally solubilized (*i.e.* no fractionation) within the bile salt mixed micelles, with a probable additional contribution of water soluble products for fatty acids ≤ C8. The present model provides a significant improvement in comparison with models which assume an average lipolysis rate with a better representation of the intestinal lipid digestion mechanisms.

Acknowledgements

This work was supported by the Institut National de la Recherche Agronomique and the Institut Carnot QUALIMENT (France). The authors are involved in the Food and Agriculture COST (European Cooperation in Science and Technology) Action FA1005 ‘Improving health properties of food by sharing our knowledge on the digestive process (INFOGEST)’.

430

431 **Nomenclature**

Symbols	***Meaning***
A_{TAG}	Interfacial area of the oil droplets (m^2)
A_{FA_i}	Interfacial area occupied by the i^{th} FA residue (m^2)
d_{32}	Surface weighted mean droplet diameter (nm)
k_{FA_i}	Lipolysis rate constant of the i^{th} FA residue (mg m^{-2} min^{-1})
$f_{FA_i}^{mic}$	Micellar mass fraction of the i^{th} FA
M_{FA_i}	Molecular mass of the i^{th} FA (g mol^{-1})
m_{TAG}	Mass of TAG (mg)
$m_{FA_i}^{lip}$	Mass of the i^{th} FA residue in oil droplets (mg)
$m_{FA_i}^{mic}$	Mass of the i^{th} FA in micellar phase (mg)
$n_{FA_i}^{lip}$	Quantity of the i^{th} FA residue in oil droplets (mmol)
$n_{FA_i}^{mic}$	Quantity of the i^{th} FA in aqueous phase (mmol)
t	Time (min)
ρ	Average mass density of TAG (mg mm^{-3})
α	Fraction of FA residue coming from LCT
1-α	Fraction of FA residue coming from MCT

432

433

References

Akanbi, T. O., Sinclair, A. J., & Barrow, C. J. (2014). Pancreatic lipase selectively hydrolyses DPA over EPA and DHA due to location of double bonds in the fatty acid rather than regioselectivity. *Food Chemistry*, *160*, 61–66.

Armand, M., Borel, P., Ythier, P., Dutot, G., Melin, C., Senft, M., … Lairon, D. (1992). Effects of droplet size, triacylglycerol composition, and calcium on the hydrolysis of complex emulsions by pancreatic lipase: an in vitro study. *The Journal of Nutritional Biochemistry*, *3*, 333–341.

Armand, M., Pasquier, B., André, M., Borel, P., Senft, M., Peyrot, J., … Lairon, D. (1999). Digestion and absorption of 2 fat emulsions with different droplet sizes in the human digestive tract. *The American Journal of Clinical Nutrition*, *70*(6), 1096–1106.

Berger, M., & Schneider, M. P. (1991). Lipases in organic solvents: The fatty acid chain length profile. *Biotechnology Letters*, *13*(9), 641–645.

Berton, C., Genot, C., & Ropers, M.-H. (2011). Quantification of unadsorbed protein and surfactant emulsifiers in oil-in-water emulsions. *Journal of Colloid and Interface Science*, *354*(2), 739–748.

Bottino, N. R., Vandenburg, G. A., & Reiser, R. (1967). Resistance of certain long-chain polyunsaturated fatty acids of marine oils to pancreatic lipase hydrolysis. *Lipids*, *2*(6), 489–493.

Carriere, F., Barrowman, J. a, Verger, R., & Laugier, R. (1993). Secretion and contribution to lipolysis of gastric and pancreatic lipases during a test meal in humans. *Gastroenterology*, *105*(3), 876–888.

Desnuelle, P., & Savary, P. (1963). Specificities of Lipases. *Journal of Lipid Research*, *4*(9), 369–384.

Freeman, C. P. (1969). Properties of fatty acids in dispersions of emulsified lipid and bile salt and the significance of these properties in fat absorption in the pig and the sheep. *The British Journal of Nutrition*, *23*(2), 249–263.

Giang, T. M., Le Feunteun, S., Gaucel, S., Brestaz, P., Anton, M., Meynier, A., & Trelea, I. C. (2015). Dynamic modeling highlights the major impact of droplet coalescence on the in vitro digestion kinetics of a whey protein stabilized submicron emulsion. *Food Hydrocolloids*, *43*(2015), 66–72.

Golding, M., & Wooster, T. J. (2010). The influence of emulsion structure and stability on lipid digestion. *Current Opinion in Colloid & Interface Science*, *15*(1-2), 90–101.

Golding, M., Wooster, T. J., Day, L., Xu, M., Lundin, L., Keogh, J., & Clifton, P. (2011). Impact of gastric structuring on the lipolysis of emulsified lipids. *Soft Matter*, *7*(7), 3513–3523.

Hofmann, A. F. (1963). The behavior and solubility of a number of pure monoglycerides in dilute, micellar bile-salt solution. *Biochimica et Biophysica Acta*, *70*, 306–316.

Jurado, E., Camacho, F., Luzón, G., Fernández-Serrano, M., & García-Román, M. (2008). Kinetics of the enzymatic hydrolysis of triglycerides in o/w emulsions. *Biochemical Engineering Journal*, *40*(3), 473–484.

Kenmogne-Domguia, H. B., Meynier, A., Viau, M., Llamas, G., & Genot, C. (2012). Gastric conditions control both the evolution of the organization of protein-stabilized emulsions and the kinetic of lipolysis during in vitro digestion. *Food & Function*, *3*(12), 1302–1309.

Lawson, L. D., & Hughes, B. S. (1988). Human absorption of fish oil fatty acids as triacylglycerols, free acids, or ethyl esters. *Biochemical and Biophysical Research Communications*, *152*(1), 328–335.

Li, Y., & McClements, D. J. (2010). New mathematical model for interpreting pH-stat digestion profiles: impact of lipid droplet characteristics on in vitro digestibility. *Journal of Agricultural and Food Chemistry*, *58*(13), 8085–8092.

Mukherjee, K. D., Kiewitt, I., & Hills, M. (1993). Substrate specificities of lipases in view of kinetic resolution of unsaturated fatty acids. *Applied Microbiology and Biotechnology*, (40), 489–493.

Sek, L., Porter, C. J. H., Kaukonen, A. M., & Charman, W. N. (2002). Evaluation of the in-vitro digestion profiles of long and medium chain glycerides and the phase behaviour of their lipolytic products. *The Journal of Pharmacy and Pharmacology*, *54*(1), 29–41.

Smith, M. E., & Morton, D. G. (2010). *The digestive system*. (New York by Churchill Livingstone, Ed.) (2nd ed.).

Tzocheva, S. S., Kralchevsky, P. A., Danov, K. D., Georgieva, G. S., Post, A. J., & Ananthapadmanabhan, K. P. (2012). Solubility limits and phase diagrams for fatty acids in anionic (SLES) and zwitterionic (CAPB) micellar surfactant solutions. *Journal of Colloid and Interface Science*, *369*(1), 274–286.

Verger, R., & de Haas, G. H. (1976). Interfacial enzyme kinetics of lipolysis. *Annual Review of Biophysics and Bioengineering*, *5*, 77–117.

Verger, R., Mieras, M. C. E., & de Haas, G. H. (1973). Action of Phospholipase A at Interfaces. *The Journal of Biological Chemistry*, *248*, 4023–4034.

Yang, L. Y., Kuksis, A., & Myher, J. J. (1990). Lipolysis of menhaden oil triacylglycerols and the corresponding fatty acid alkyl esters by pancreatic lipase in vitro: a reexamination. *Journal of Lipid Research*, *31*(1), 137–147.

Ye, A., Cui, J., Zhu, X., & Singh, H. (2013). Effect of calcium on the kinetics of free fatty acid release during in vitro lipid digestion in model emulsions. *Food Chemistry*, *139*(1-4), 681–688.

506 Zhu, X., Ye, A., Verrier, T., & Singh, H. (2013). Free fatty acid profiles of emulsified lipids
507 during in vitro digestion with pancreatic lipase. *Food Chemistry*, *139*(1-4), 398–404.

508

509 **Figure Captions**

510

511 **Fig 1.** Lipolysis of MCT (squares) and LCT (triangles) during intestinal digestion (A).
512 Surface weighted mean diameters, d_{32}, (circles) and interfacial areas (diamonds) of oil
513 droplets (B). Solid lines are guide for the eyes. Means and standard deviations (smaller than
514 symbol size) were calculated over 3 replicates.

515

516 **Fig 2.** Bioaccessibility of individual lipolysis products (lines are guides for eyes). Means and
517 standard deviations were calculated over 3 replicates.

518

519 **Fig 3.** Comparison between calculated and experimental evolutions of the MCT, LCT, and
520 bioaccessible product masses during intestinal digestion. Symbols are means over 3 replicated
521 experiments (squares for MCT, triangles for LCT). Solid lines show the mass evolution
522 calculated using the model. Dotted lines show the asymptotic values calculated using the
523 model.

524

525 **Fig 4.** Lipolysis rate constants for the different fatty acid residues according to the carbon
526 chain length (expressed as normalized values relatively to C18:1 n-9). Crosses represent the
527 values determined in this study by model fitting. Squares correspond to values reported by
528 Berger & Schneider (1991). The circle and the triangle for C22:6 n-3 were estimated from the
529 studies of Mukherjee *et al*. (1993) and Yang et al. (1990), respectively.

530

531 **Fig 5.** Evolution of the interfacial areas (normalized values) occupied by each fatty acid
532 residue during intestinal digestion (A). Zoom on the first 15 min (B).

533

534 **Figure 1**

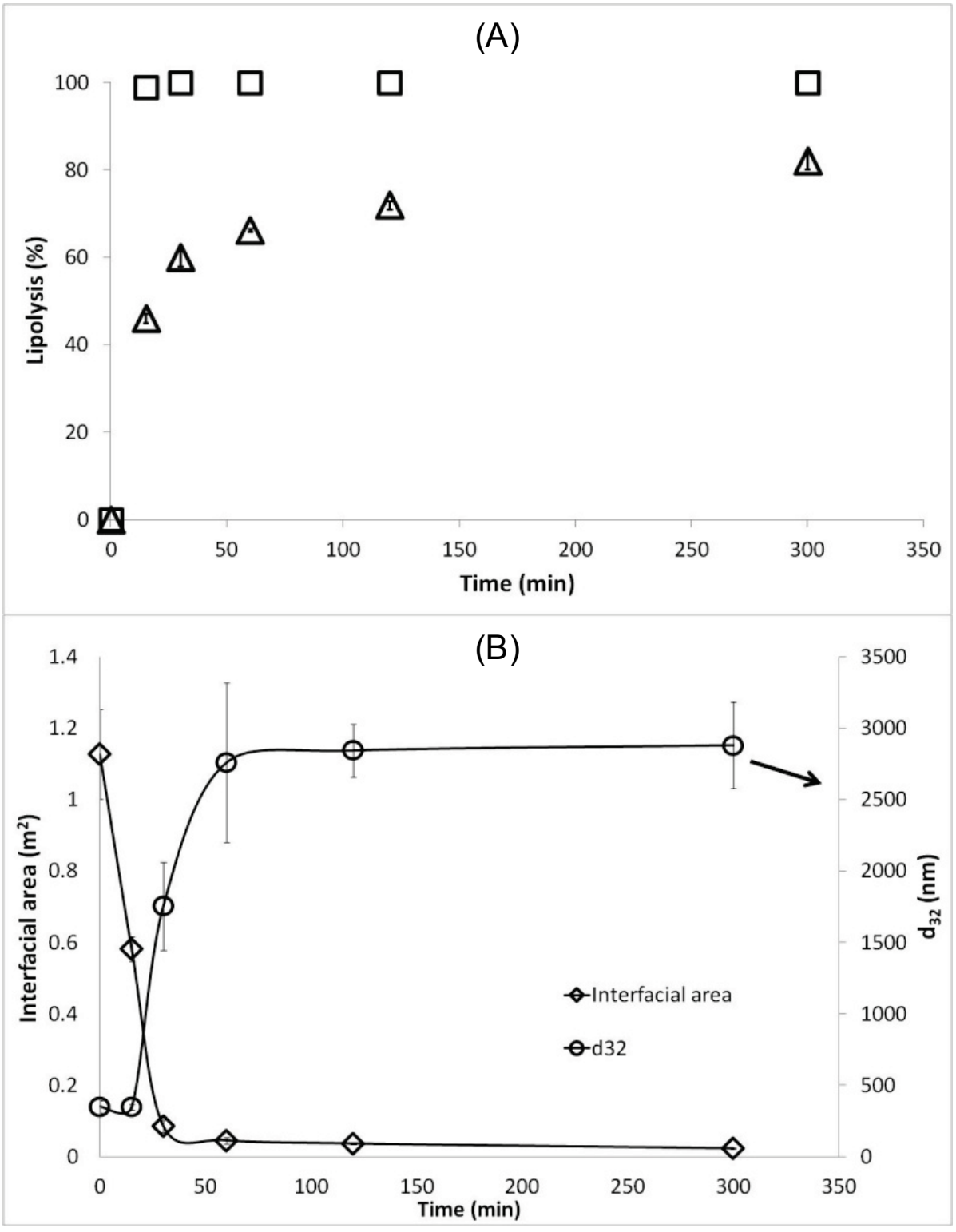

535

536

537

538 **Figure 2**

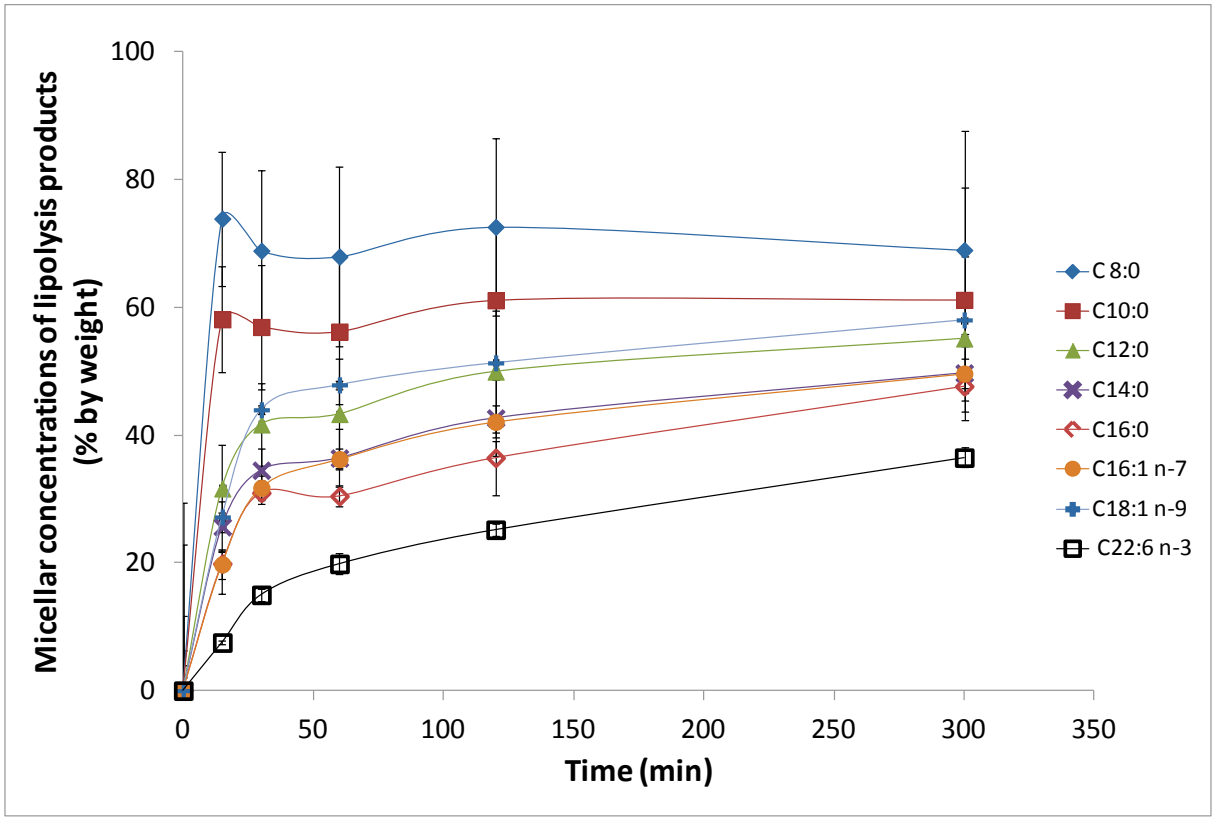

539
540

541

542

543 **Figure 3**

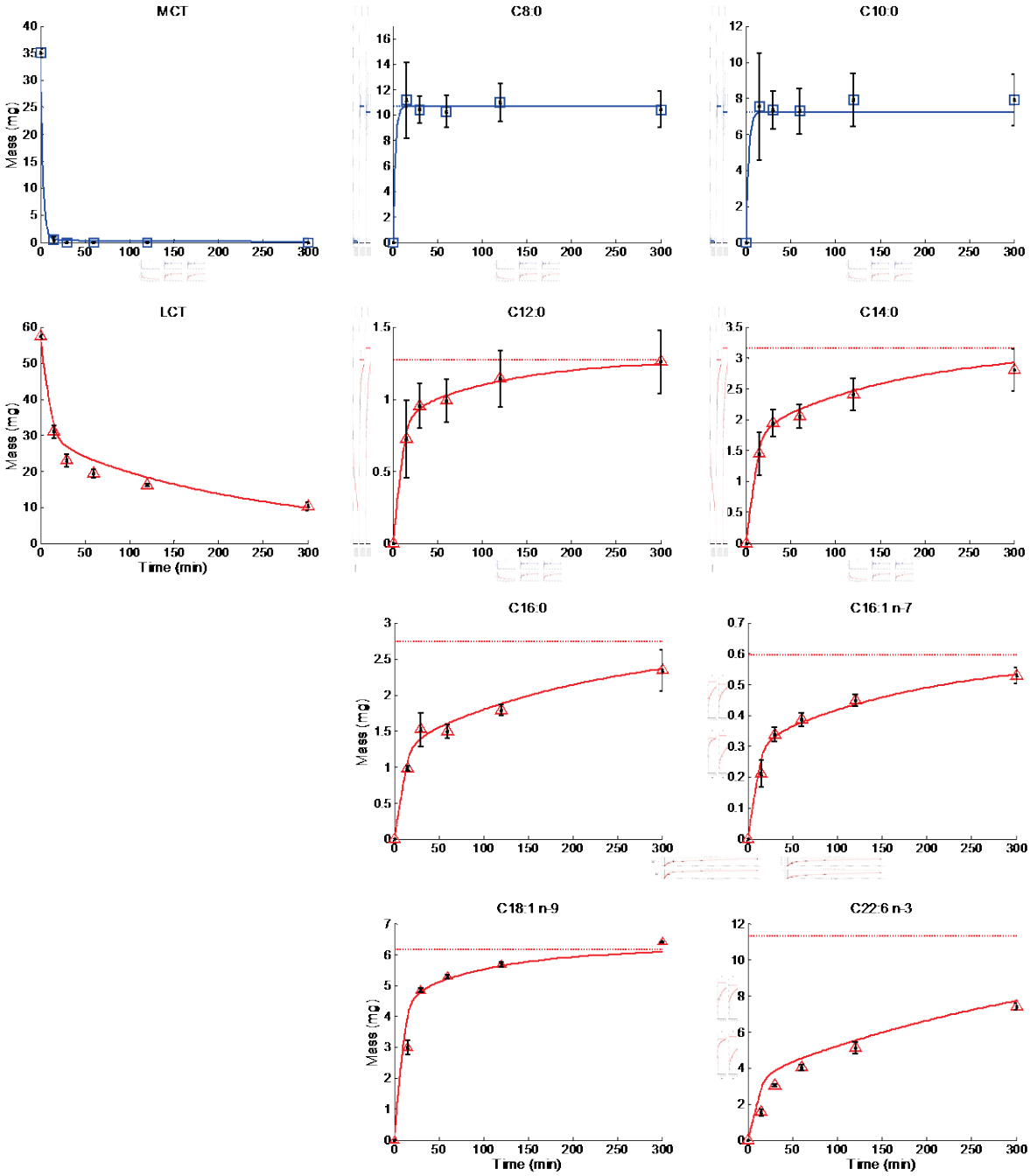

544
545

546 **Figure 4**

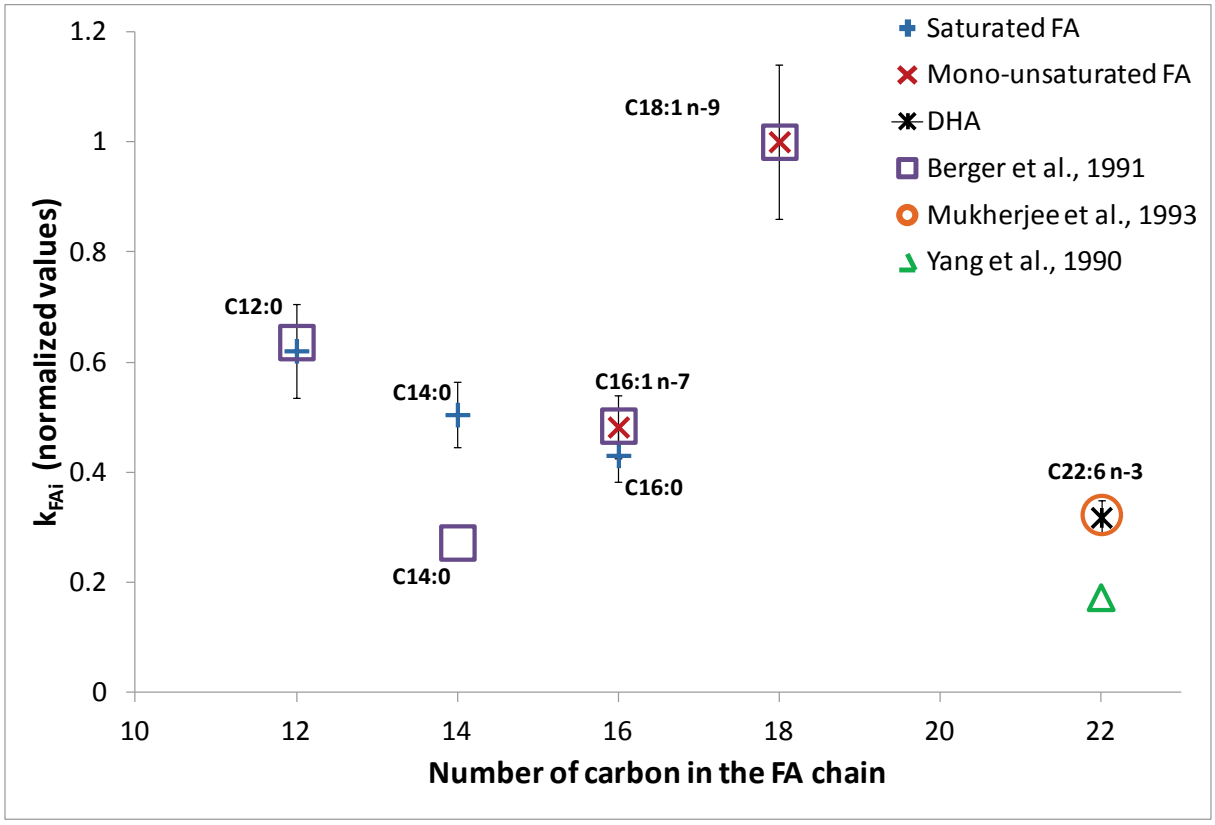

547

548

549

550 **Figure 5**

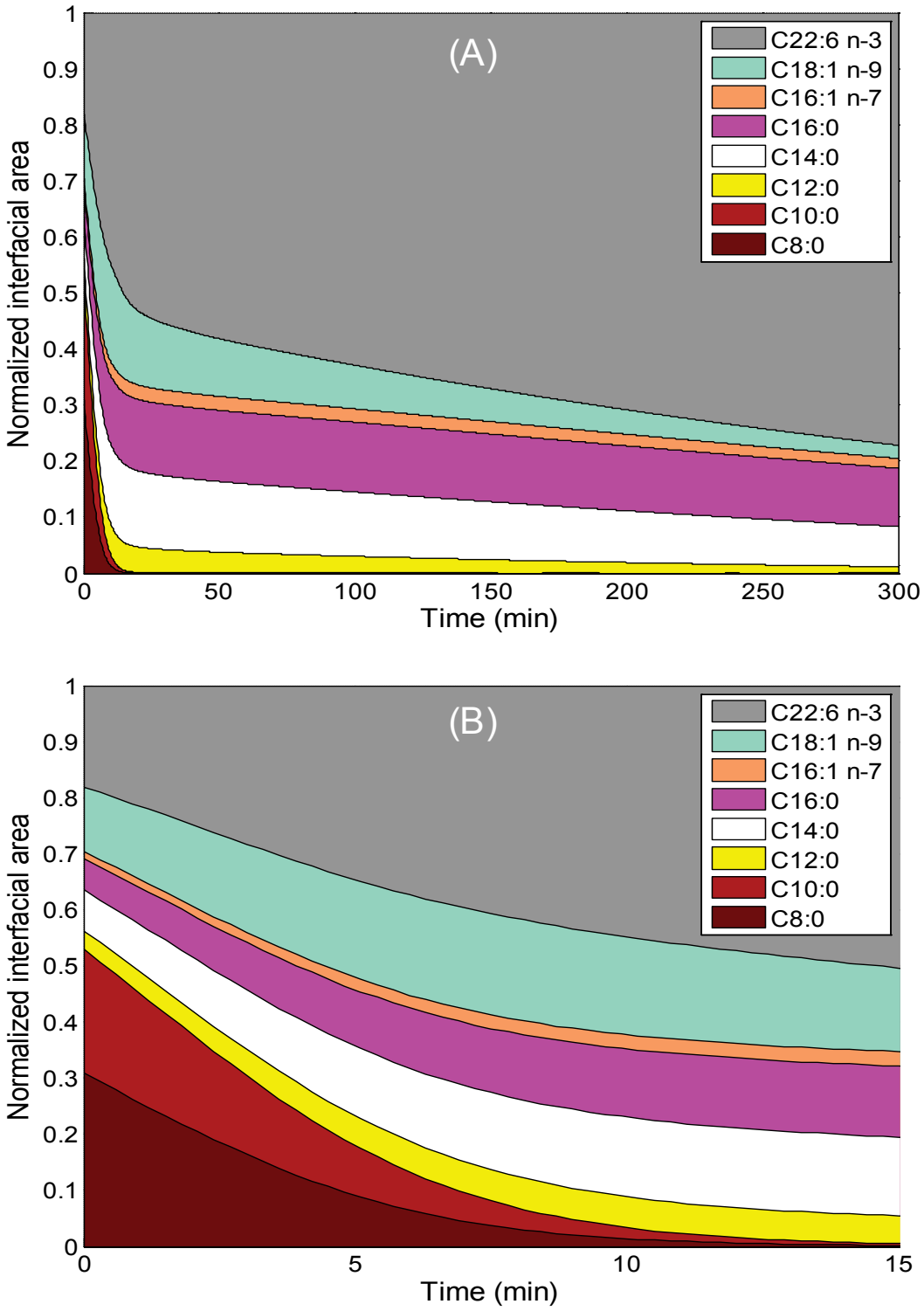

551

552 **Table 1.** Fatty acid composition of the native emulsion which was made of a mixture of MCT

553 and LCT (37.5 and 62.5 % by weight, respectively).

Fatty acid	TAG composition		Origin of each FA	
	Mean of 3 replicates (% by weight)	STD of 3 replicates (% by weight)	Fraction coming from LCT α_{FA_i}	Fraction coming from MCT 1-α_{FA_i}
C8:0	19.76	0.71	0.02	0.98
C10:0	16.89	0.33	0.05	0.95
C12:0	2.98	0.20	0.93	0.07
C14:0	7.36	0.09	0.97	0.03
C16:0	6.40	0.13	0.92	0.08
C16:1 n-7	1.39	0.07	0.99	0.01
C18:1 n-9	14.41	0.14	0.98	0.02
C22:6 n-3	26.47	0.10	1.00	0.00
Other FA	4.31	1.72	0.89	0.11

554

555

556

557 **Table 2.** Results of the parameter estimation for the lipolysis rate k_{FA_i} and the micellar

558 fraction $f_{FA_i}^{mic}$ for each fatty acid.

Fatty acid	k_{FA_i} (mg min^{-1} m^{-2})		$f_{FA_i}^{mic}$	
	Value	STD	Value	STD
C8:0	10*		0.70	0.01
C10:0	10*		0.56	0.01
C12:0	1.93	0.16		
C14:0	1.57	0.11		
C16:0	1.34	0.10		
C16:1 n-7	1.50	0.11		
C18:1 n-9	3.11	0.25		
C22:6 n-3	0.99	0.06		

559 (*) minimum value providing a complete hydrolysis of MCT in 15 min.

560